Micronewton nanofiber force sensor using Brillouin scattering

Adrien Godet, Jacques Chretien, Kien Phan Huy, Jean-Charles Beugnot

Micronewton nanofiber force sensor using Brillouin scattering

ADRIEN GODET, JACQUES CHRETIEN, KIEN PHAN HUY AND JEAN-CHARLES BEUGNOT*

Institut FEMTO-ST, UMR 6174 CNRS, Universite Bourgogne Franche Comte, Besancon, France
**jc.beugnot@femto-st.fr*

Abstract: We present a new class of force sensor based on Brillouin scattering in an optical nanofiber. The sensor is a silica nanofiber of few centimeters with submicron transverse dimension. This extreme form factor enables one to measure forces ranging from 10 μN to 0.2N. The linearity of the sensor can be ensured using the multimode character of the Brillouin spectrum in optical nanofibers. We also demonstrated non-static operation and a competitive signal to noise ratio as compared to commercial resistive force sensor.

1. Introduction

Force measurement is a major technological challenge as new applications are identified in air/spacecraft industries, electric power facilities or micro and nanotechnologies for biology [1–5]. Force measurement systems are typically based on resistive, piezo-resistive, capacitive, piezoelectric, magnetic, inductive, or optic measurement methods [6–8]. While each has benefits and drawbacks, fiber optical sensors are uniquely suited while electromagnetic immunity and high resolution are required, or chemically aggressive and conductive liquids environments are present [9]. The resolution and dynamic range of different force measurement systems are reported in Fig. 1. Notice that for every technology there is a compromise between resolution and dynamic range. Most optical fiber sensors, as shown in green and blue in Fig. 1, are using either fiber Bragg gratings (FBG), Fabry–Perot or another interferometric scheme. They offer both a broad detection range and a high sensitivity that make them very attractive for applications such as earthquake monitoring or automation systems [10]. Concurrently, Brillouin fiber sensors were developed for distributed sensing. They were rarely used as force measurements. However, they offer a major benefit which is the absence of grating or interferometer manufacturing, because they use the interaction between light and an acoustic wave that behaves as a moving Bragg reflector. As shown in blue in Fig. 1, their use is limited to milli-Newton force measurements.

With the development of MEMS a new class of high sensitive sensors have come of age, as they benefit from smaller dimensions, their sensitivity can range from micro to tens of nano Newtons, as shown in grey and purple in Fig. 1. MEMS sensors dynamic range covers tens of milli-Newton to dozen Newtons with performances no single mode fiber (SMF) based Fiber could ever reach. Achieving the higher sensitivity requires 3-D scale reduction. In the case of SBS fiber based force sensors, it limits the efficiency since long distance of interaction are needed to provide strong Brillouin scattered signal. Due to the small transverse dimension combined with the large longitudinal dimension, the optical nanofiber (ONF) possesses the requisite sensitivity at scale thanks to the reduced transverse dimension while providing strong Brillouin scattered signal thanks to the longer longitudinal dimension. Consequently, it's possible to increase force sensitivity by several orders of magnitude compared to fiber force sensor as Bragg grating in conventionally sized fibers. [11–14].

In our previous work, we demonstrated high sensitivity longitudinal stress measurements using Brillouin scattering in ONFs [15]. Knowing the nanoscale cross-section of nanofibers (the waist part of the tapered fiber), it paves the way for a new class of highly sensitive force sensors whose

sensitivity scales inversely with the cross-section. In Fig. 1, we report few of our experimental results, described below, that demonstrate that this new class of sensors covers a large area of measurement sensitivities and dynamic range.

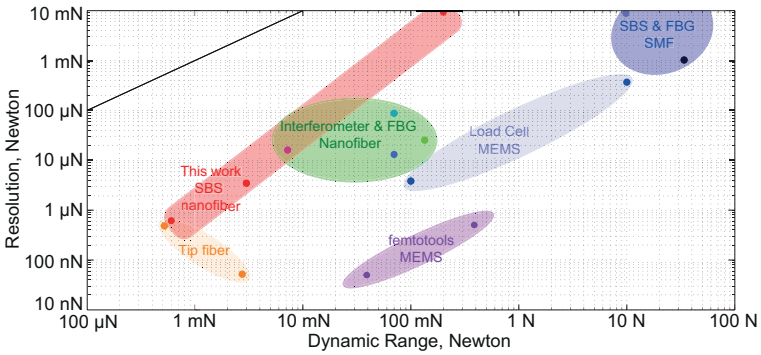

Fig. 1. Comparison of key force sensor figure of merit (resolution and dynamical range) for this work, for state of the art optical fiber force sensor (SBS and FBG in single mode fiber [9, 16]), not limited to fiber based sensor (Load cell MEMS [17] and femtotools [18]) and for previous results obtain with tapered optical fiber [19–22]. The black line represent the limit resolutions equal to dynamic. In comparison with other nanofiber platforms, our solution with Brillouin scattering show higher resolution and much lower losses at the same time. And the inline measurement without functionalisation of fiber open new possibility in the region (1um resolution, 1mN dynamic range) in complementary to fiber tip sensor [23, 24].

The article is organized as follows. We first give the theoretical background of the nanofiber Brillouin sensor. We explain how high sensitivity is obtained and describe the experimental setup. We then present the measurements obtained with this setup, and how the sensitivity evolves with the diameter of the nanofiber and the operating range of our sensors. In the third section, we demonstrate how to ensure the linearity of the sensor response through several examples. Finally, we show that our sensors are not limited to the static regime and compare the sensor signal-to-noise ratio with a commercial strain gauge sensor.

2. Optical force sensor

The force sensor is built around an optical nanofiber (ONF) obtained by drawing a standard optical fiber using the well-known heat-brush technique until its diameter reaches the nanoscale [25, 26] as shown in Fig. 1(a). When a pump laser light propagates in the ONF (in blue), it interacts with the acoustic waves supported by the ONF. Those acoustic waves behave as a moving mirror and reflect light (pink) via Brillouin scattering. This backscattered Stokes light is shifted in frequency by the Doppler effect. This shift is therefore related to the elastic waves velocity. If a force is applied to one end of the fiber (purple arrow), the nanowire under stress will be strained. The yellow to red color gradient shows how the stress and strain are distributed along the tapered fiber. Because of the strong tapering ratio (125 µm to a few hundreds of a nanometer) the strain is much stronger in the center part call the optical nanofiber [27].

Since the strain alters the acoustic wave's velocity, and causes a variation of the Brillouin frequency shift, we can deduce the applied force by measuring this frequency shift. In our setup shown in Fig. 2, the optical nanofiber is held securely with clamps. A commericial resistive force sensor (ME-systeme KD-78) allows us to measure the longitudinal force that we apply due to motorized translation stages (Newport XML210). The frequency shift is measured through a

heterodyne setup. A part of the pump beam is mixed with the backscattered beam to produce an optical beat measured with an radiofrequency electric spectrum analyser. The frequency shifts for each acoustic mode are retrieved with respect to the measured force using a lorentzian fit [28].

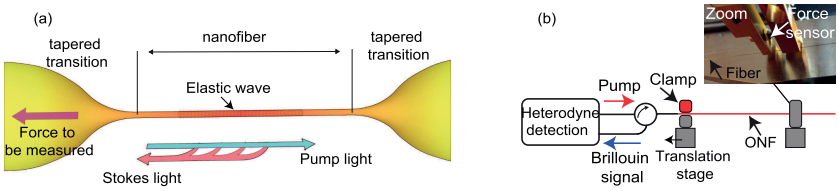

Fig. 2. (a) Schematic of the nanofiber force sensor. (b) Experimental setup for measuring the longitudinal force as a function of the Brillouin spectrum. Inset picture: ME-systeme KD-78 resistive force sensor completed with an amplifier GSV-2TSD-DI

One of the most challenging specification to meet for an optical force sensor is high sensitivity. ONF uses the expression of the longitudinal normal strain to improve sensitivity

$$\sigma_{zz} = \frac{F_{zz}}{S}, \tag{1}$$

where F_{zz} is a longitudinal force and S is the cross-sectional area over which the force is applied [29]. This expression shows how a very small force F_{zz} can result in relatively strong stress σ_{zz} providing that the cross-sectional area S is small. Additionally, the approximated 1-D Hooke's law tells us that the longitudinal stress represented as

$$\sigma = E\epsilon, \tag{2}$$

where E is Young modulus (73 GPa in silica) and ϵ_{zz} is the longitudinal tensile strain. In this case, for a sufficiently small cross-sectional area, a small longitudinal force can lead to a measurable tensile strain ϵ_{zz}. This is schematically illustrated by the figure 2(a), where a tapered optical fiber is depicted. A longitudinal force is applied at one end. Most of the strain appears in the central region highlighted in red where the cross sectional area is the smallest [15]. In a standard optical fiber, the Brillouin frequency shift varies linearly with an applied tensile strain ϵ_{zz} inferior to 2% and a normalized Brillouin strain coefficient that is given by

$$C_\epsilon = \frac{1}{\nu_B}\frac{\partial \nu_B}{\partial \epsilon_{zz}}, \tag{3}$$

where ν_B, Brillouin frequency shift. For a SMF-28 it is typically 4.25 [30]. Combining eq 1, 2 and 3 we can compute the sensitivity S that gives the Brillouin Frequency shift for a given applied force,

$$S = \frac{\partial \nu_B}{\partial F_{zz}} = 4\frac{\nu_B C_\varepsilon}{\pi E d^2}, \tag{4}$$

where d is the diameter of the silica nanofiber. This expression scales inversely with the square of the nanofiber diameter which means that reducing an optical fiber diameter from 125μm to few hundreds of a nanometer could increase the sensitivity by four or more orders of magnitude.

Although the benefit from reducing the diameter of the fiber is obvious, it also raises questions. In order to make a usable sensor, it is necessary to discriminate the light scattered in the ONF from that scattered in the standard fibers of the optical setup. Also the scattered light must be strong enough to allow detection and measurement of the Brillouin frequency shift. This is only possible if the acousto-optic interaction is strong which requires low optical losses, long (few centimeters) ONF and strong light confinement. We will see in the next paragraph, through the experimental results that an ONF can fulfill all those requirements.

3. Sensitivity enhancement

Brillouin spectra were measured with a ONF of 630 nm diameter with different applied force going from 0 to 611 μN as shown by Fig. 3(a). The ONF is 40 mm long and the losses are below 0.2 dB at telecommunication wavelength. We observe many acoustic resonances, such as hybrid acoustic waves (HAW) in the range (8 GHz-9 GHz), the resonances due to the taper transitions (9 GHz to 10.8 GHz) and the untapered optical fibers (10.8 bGHz). The presence of many resonances is due to the fact that in an ONF the acoustic waves behave as modes, each having its own velocity and therefore Brillouin frequency shift. It enables to discriminate easily the contribution of the ONF to the Brillouin spectrum and thus eliminates the need for active or passive stabilization of the fibers belonging to the rest of the heterodyne circuit. Those resonances experience a blue frequency shift that increases with the applied force. The main resonance just below 11 GHz comes from the single mode fibers contribution to the Brillouin spectrum (See Fig. 2). As those fibers belong to the heterodyne setup, no force is applied to them. It results in the absence of frequency shift for the 11 GHz resonance. Similar measurements were performed

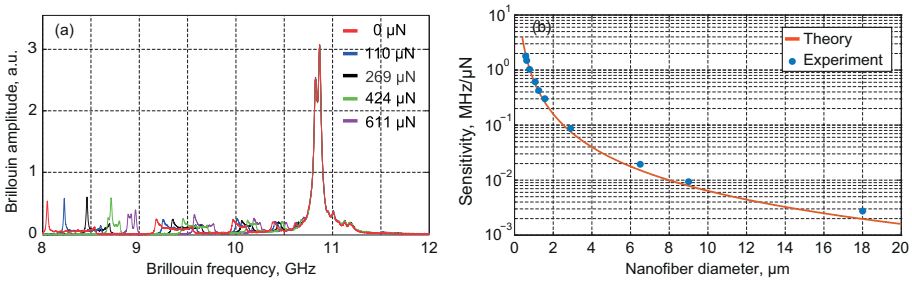

Fig. 3. (a) Experimental backscattering Brillouin spectrum in a ONF with a diameter of 630nm a length of 40 mm for 5 different applied forces. (b) frequency sensitivity normalized to μN as a funtion of the nanofiber diameter, theory (red), experiment (blue point).

for 10 different ONF diameters ranging from 18 µm to 630nm. The geometric parameters of tapered optical fibers as nanofiber diameter and homogeneity are precisely estimated by Brillouin spectroscopy [28]. For each diameter, the sensitivity is measured for strain smaller than 2% for 9-10 GHz Hybrid Acoustic Waves (HAW) resonances [15] and reported in Fig. 3(b). The experiment data were fitted using equation 4. A force sensitivity around 1.9 MHz/μN is reached for an ONF of diameter 630 nm. This means that force sensitivity is higher by more than five orders of magnitude compared to an untapered fiber [30]. The analytical model is in good agreement with the experimental measurements and the small differences can be explained by small temperature variations.

4. Range

In order to explore the potential operating range of a family of force sensors based on optical nanofibers, we performed measurements with ONF of diameters ranging from 580 nm to 18 microns. All the ONFs were 40 mm long with losses less than 0.2 dB. The results are shown in Fig. 4, where the Brillouin frequency shifts are plotted as a function of applied force (the total nanofiber elongation is shorter to 2% to maintain the linear regime). Note that logarithmic scales were used to better represent the wide operating range of our sensor family. This shows that we could in principle make measurements of few tens of micrometers and even reach values lower than the reliability limit of our commercial strain gauge (blue area). We also note that for a diameter of 18 μm, we can measure forces approaching 0.2 N. This limit can be pushed

back since nanofibers of diameters going up to hundreds of micron could be developed with further manufacturing effort. The improvement in sensitivity for smaller diameters is again

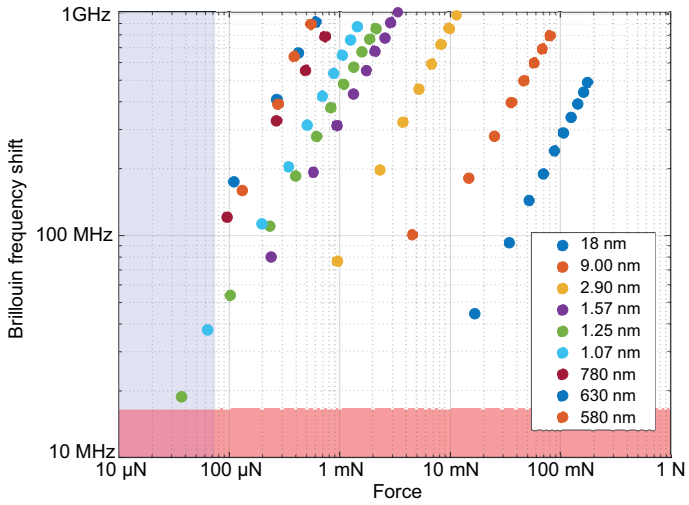

Fig. 4. Measurements of Brillouin frequency shift as a function of applied force for different diameter of tapered optical fibres ranging from 580 nm to 18 μm. Force and frequency are plotted in log scale. Blue area for measurements inferior to 70 μN is where our measurements are less reliable due to the strain gauge limitation. The pink area represents the limits of our ability to measure Brillouin frequency shifts with Lorentzian fits.

confirmed by Fig. 4, as the measurements from small ONF diameters correspond to small forces and measurements associated with large diameters to large forces. However, a number of details raise questions. The measurements for the 580 and 630 nm diameters appear to correspond to curves that would intersect. The same is true for the 1.07 and 1.25 μm diameters. Also, the ONF points of diameter 9 μm seem to show an inflection. We will explain these observations through the following three examples in the following.

5. Linearization

In this paragraph, we will focus on measurements obtained for ONF with diameters 610 nm, 855 nm and 1570 nm. The results are shown in Fig. 5(a-c), where the Brillouin spectrum are plotted in false color with respect of applied force. In those cases, the ONF were stretch until 6% showing clear sensitivity variation from one resonance to the other as well as nonlinear behaviour. Fig. 5(a) for example, shows the surface acoustic waves (SAW) between 5 and 6.5 GHz contribution almost crossing each other for higher applied force. The HAW resonance starting here at 10 GHz in Fig. 5(c) is also a great example of nonlinearity. It can be seen that the 10 GHz and 11 GHz resonances move closer together as the applied force increases, then move apart for forces exceeding 5 mN. The nonlinear behavior results from both the third order elastic constant and from the acoustic modal dispersion [15]. A common point of Fig. 5(a-c) is the presence of three resonances corresponding to three acoustic modes. For each resonance from Fig. 5(a-c), we interpolated the Brillouin frequency variation as a function of the applied force

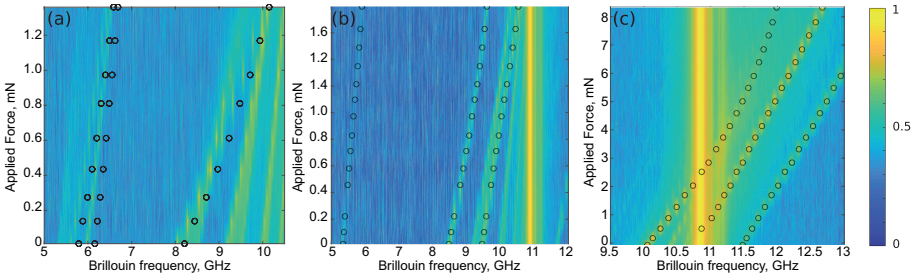

Fig. 5. (a), (b) and (c) In false color, experimental Brillouin spectrum with respect of the applied Force measured with the strain gauge for a 1570 nm, 855 nm and 610 nm diameter ONF respectively. The Circle represent the theoretical model from [15].

by a third order polynomial. The three obtained polynomials form a 3x3 system

$$\begin{pmatrix} \Delta\nu_0 \\ \Delta\nu_1 \\ \Delta\nu_2 \end{pmatrix} = \begin{pmatrix} m_{11} & m_{12} & m_{13} \\ m_{21} & m_{22} & m_{23} \\ m_{31} & m_{32} & m_{33} \end{pmatrix} \begin{pmatrix} F \\ F^2 \\ F^3 \end{pmatrix}, \tag{5}$$

with the coefficient $(m_{ij})_{\{1,2,3\}^2}$ forming the matrix M. Thanks to the acoustic mode dispersion, each Brillouin frequency shift varies differently enough for equation 5 to be invertible. The matrix M inversion allows us to obtain F_{llin} as a linear combination of the Brillouin frequency shift of each resonance.

$$F_{\text{lin}} = a_{01}\Delta\nu_0 + a_{02}\Delta\nu_1 + a_{03}\Delta\nu_2, \tag{6}$$

where the weights a_{01}, a_{02} and a_{03} are the coefficient of the first line of the inverted matrix M^{-1}. We plot in Fig. 6(a), the measured F_{lin} with respect to the applied force measured with the strain gauge for the three measurements shown Fig. 5. The measurements from the blue, orange and green dots coming from the 1570 nm, 855 nm and 610 nm diameters ONFs respectively show excellent linearity (gray line). We thus demonstrate that the quadratic and cubic contribution of the nonlinearity are well compensated by the contibution of the second and third resonance frequency shifts. We also show that interpolating the measured frequency shifts with cubic polynomials, neglecting the fourth order coefficient is a valid approximation. The same results, are also shown in log scale in Fig. 6(b), to better illustrate the range covered by the three experiments. Measurements ranging from 20 μN to 7 mN confirm that the linearization does not affect the range while maintaining a good sensitivity.

6. Non-static regime and Signal-to-Noise Ratio

One of functionalities for a force sensor is the ability to measure in a non-static regime. This could be usefull if a control loop mechanism employing feedback is used to dynamically maintain or alter the applied force. Also for this kind of application a good signal-to-noise ratio is required. To test the ability of our sensor to perform these kind of measurements, we fabricated an ONF with a diameter of 885 nm with an homogeneous section of 40 mm length. We isolated a Brillouin resonances at 8 GHz corresponding to hybrid elastic mode (L(0,2)) which is one of the most sensitive to longitudinal strain. On the top of Fig 7(a), we represent the stretching pattern applied to the ONF as a function of time. At each cycle, the ONF is stretched by a distance increased of 100 µm and then released to its inital state. We sequentially launch 15 cycles manually until a maximum stretch of 1500 µm is reached. As shown in Fig. 7(b) The force applied by the fiber stretching is measured by both the resistive force sensor (blue) and Brillouin scattering (red).

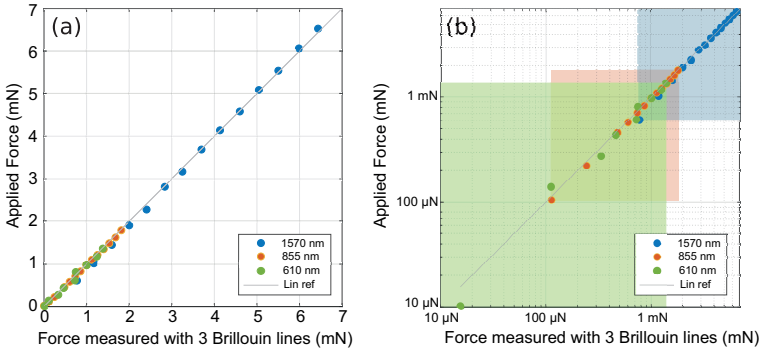

Fig. 6. (a) In false color, Brillouin spectrum computed with Finite-Element Method for different ONF diameters. Black line: 855 nm diameter. (b) Brillouin frequencies for the TR21 (red), L01, L02 and L03 (blue) acoustic mode resonances for a 855 nam diameter ONF with respect to strain. In gray, same resonances without modal dispersion.

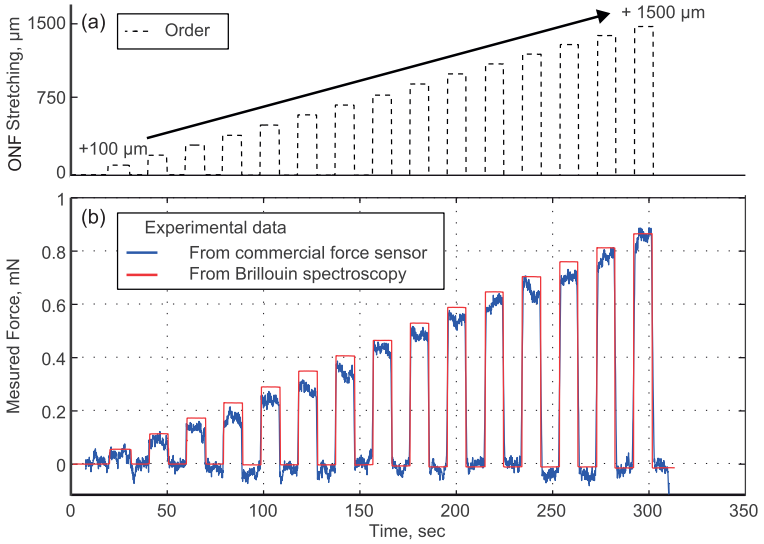

Fig. 7. (a) Stretching pattern applied to the ONF for non-static measurement. (b) Experimental force measurement from commercial strain gauge in blue and the ONF of diameter of 885 nm optical force measurement in red.

The red curve showing the response of the optical sensor clearly presents a better signal-to-noise ratio. This is particularly evident for the first cycle, for which the commercial strain gauge has difficulty in producing a clean measurement. We can also guess from the slopes that the optical sensor has a better frequency response. To evaluate the noise performance, we have plotted the distribution of normalized measurements around the mean value for each of the sensors in Fig. 8(a). The distribution produced by the resistive commercial sensor in blue shows a broad Gaussian distribution (standard deviation of 0.0167) while the normalized distribution obtained with the optical sensor is mostly concentrated in the central bin. By reducing the size of the bins by a factor of 90, the normalized distribution of the optical measurements can be represented again and show a Gaussian of standard deviation 2.3×10^{-4}. This confirms the better signal-to-noise performance of our sensor by nearly two orders of magnitude. In order to confirm

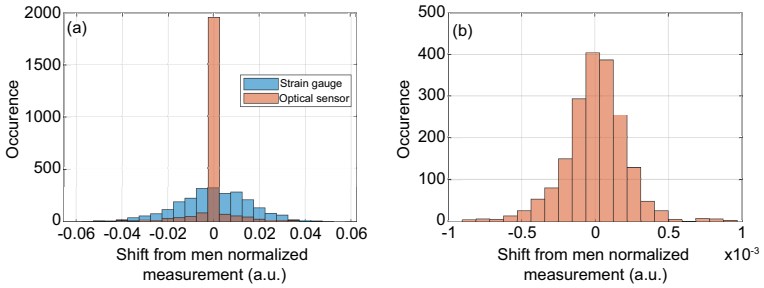

Fig. 8. (a) Measurements distribution around the mean force reported in fig 7(a) for commericial resistive sensor (blue) and optical sensor (light brown). (b) Optical force measurements distribution around the mean force reported in fig 7(a) with proper scale.

the good behavior of the optical sensor in dynamic regime compared to the commercial sensor, we have computed the fourrier transforms of the measurements from Fig 7(b) and plotted the spectrum of the optical sensor measurement in blue and the one from the commercial strain gauge in light brown as shown in Fig. 9. Although the measurement cycle were performed manually at a low frequency rate, the commercial strain gauge signal spectrum (in light brown) shows clear limitations with a cut-off around 1 kHz. Above this frequency, only noise is to be found whereas the optical sensor reveals rich harmonic content (in blue). The hysteresis effect

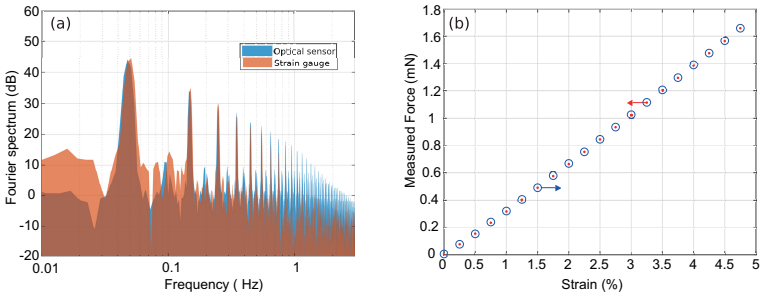

Fig. 9. Spectrum computed from dynamic measurements shown in fig 7(b). The optical sensor spectrum is in blue and the resistive commercial sensor in light brown. (b) Measured Force as a function of strain for increasing (blue circle) and decreasing force (red point).

has been considered within a cycle of increasing and decreasing applied force with the same step. The force measurement with Brillouin scattering, depicted in fig 9, demonstrate the absence of hysteresis. The better SNR performance and dynamic performance makes the ONF force sensor a better candidate for non-static measurements requested for control loop PID based force actuator application.

7. Conclusion

In conclusion, we have presented a new family of all-optical force sensors based on the measurement of Brillouin scattering in optical nano fibers. The unusual properties of these ONFs, such as low losses, 1:80,000 form factors and modal guidance of both optical and acoustic waves, give a whole new dimension to the traditional fiber Brillouin sensors. Thus we report measurements ranging from the tens of micro Newton to 0.2 N which allows this family of sensors to cover a whole new measurement range. The reduction of the diameter of the ONF to

the nanoscale over a length of a few centimeters makes it possible to reach sensitivities of the order of ten micro Newtons while preserving a significant measurement range. The linearity of the sensor, essential for a real-world application, can be obtained by taking advantage of the presence of several acoustic modes in the nanowire and their dispersion and without any specific signal processing. Finally, we have compared our sensor with a commercial resistive force sensor showing its superiority in non-static operation and showing an increase of signal-to-noise ratio close to two order of magnitude. Future improvements include packaging and surface coating in order to protect the ONF from environmental contamination.

Funding

The authors would like to acknowledge the financial support of Agence Nationale de la Recherche (ANR) via EQUIPEX+ SMARTLIGHT (ANR-21-ESRE-0040) and EIPHI Graduate School (ANR-17-EURE-0002) and Bourgogne-Franche-Comté Region.

Acknowledgement

Authors thank Maxime Zerbib for cycling force measurement.

Disclosures

The authors declare no conflicts of interest.

Data availability

Data underlying the results presented in this paper are not publicly available at this time but may be obtained from the authors upon reasonable request.

References

1. Y. Wei and Q. Xu, "An overview of micro-force sensing techniques," Sensors Actuators A: Phys. **234**, 359–374 (2015).
2. X. Liu, I. I. Iordachita, X. He, R. H. Taylor, and J. U. Kang, "Miniature fiber-optic force sensor based on low-coherence fabry-pérot interferometry for vitreoretinal microsurgery," Biomed. optics express **3**, 1062–1076 (2012).
3. P. Polygerinos, P. Puangmali, T. Schaeffter, R. Razavi, L. D. Seneviratne, and K. Althoefer, "Novel miniature mri-compatible fiber-optic force sensor for cardiac catheterization procedures," in *2010 IEEE International Conference on Robotics and Automation,* (IEEE, 2010), pp. 2598–2603.
4. D. I. Song, J. Choi, D. Kim, and M. S. Kang, "Large-capacity high-resolution optomechanical mass sensing based on free-space optical cavity," Opt. express **26**, 31567–31576 (2018).
5. P. Puangmali, H. Liu, L. D. Seneviratne, P. Dasgupta, and K. Althoefer, "Miniature 3-axis distal force sensor for minimally invasive surgical palpation," Ieee/Asme Transactions On Mechatronics **17**, 646–656 (2011).
6. M. Eichenfield, R. Camacho, J. Chan, K. J. Vahala, and O. Painter, "A picogram-and nanometre-scale photonic-crystal optomechanical cavity," nature **459**, 550–555 (2009).
7. W. H. Pernice, M. Li, D. Garcia-Sanchez, and H. X. Tang, "Analysis of short range forces in opto-mechanical devices with a nanogap," Opt. express **18**, 12615–12621 (2010).
8. J. Yu, L. Chen, H. Dong, X. Liu, H. Huang, W. Qiu, S. Huang, W. Zhu, H. Lu, J. Tang *et al.*, "Sensing and exploiting static femto-newton optical forces by a nanofiber with white-light interferometry," ACS Photonics **5**, 3205–3213 (2018).
9. Q. Liang, K. Zou, J. Long, J. Jin, D. Zhang, G. Coppola, W. Sun, Y. Wang, and Y. Ge, "Multi-component fbg-based force sensing systems by comparison with other sensing technologies: a review," IEEE Sensors J. **18**, 7345–7357 (2018).
10. W. Huang, W. Zhang, Y. Luo, L. Li, W. Liu, and F. Li, "Broadband fbg resonator seismometer: principle, key technique, self-noise, and seismic response analysis," Opt. express **26**, 10705–10715 (2018).
11. G. Tang, J. Wei, W. Zhou, M. Yang, M. Wu, and X. Xu, "A highly sensitive force sensor based on two identical fiber bragg gratings," Meas. Sci. Technol. **26**, 115203 (2015).
12. J.-L. Kou, M. Ding, J. Feng, Y.-Q. Lu, F. Xu, and G. Brambilla, "Microfiber-based bragg gratings for sensing applications: a review," Sensors **12**, 8861–8876 (2012).
13. K. M. Chung, Z. Liu, C. Lu, and H.-Y. Tam, "Highly sensitive compact force sensor based on microfiber bragg grating," IEEE Photonics Technol. Lett. **24**, 700–702 (2012).

14. W. Li, Z. Hu, X. Li, W. Fang, X. Guo, L. Tong, and J. Lou, "High-sensitivity microfiber strain and force sensors," Opt. Commun. **314**, 28–30 (2014).
15. A. Godet, T. Sylvestre, V. Pêcheur, J. Chrétien, J.-C. Beugnot, and K. Phan Huy, "Nonlinear elasticity of silica nanofiber," APL Photonics **4**, 080804 (2019).
16. S. Gao, C. Baker, L. Chen, and X. Bao, "High-sensitivity temperature and strain measurement in dual-core hybrid tapers," IEEE Photonics Technol. Lett. **30**, 1155–1158 (2018).
17. "F329 and f332 Deci-Newton Loadcell," .
18. "anoindenter, the ft-nmt04," .
19. Y. Chen, S.-c. Yan, X. Zheng, F. Xu, and Y.-q. Lu, "A miniature reflective micro-force sensor based on a microfiber coupler," Opt. Express **22**, 2443–2450 (2014).
20. W. Luo, J.-l. Kou, Y. Chen, F. Xu, and Y.-q. Lu, "Ultra-highly sensitive surface-corrugated microfiber bragg grating force sensor," Appl. Phys. Lett. **101**, 133502 (2012).
21. X. Wang, W. Li, L. Chen, and X. Bao, "Thermal and mechanical properties of tapered single mode fiber measured by ofdr and its application for high-sensitivity force measurement," Opt. express **20**, 14779–14788 (2012).
22. T. Wieduwilt, S. Brückner, and H. Bartelt, "High force measurement sensitivity with fiber bragg gratings fabricated in uniform-waist fiber tapers," Meas. Sci. Technol. **22**, 075201 (2011).
23. S. Pevec and D. Donlagic, "Miniature all-fiber force sensor," Opt. Lett. **45**, 5093–5096 (2020).
24. M. Zou, C. Liao, S. Liu, C. Xiong, C. Zhao, J. Zhao, Z. Gan, Y. Chen, K. Yang, D. Liu *et al.*, "Fiber-tip polymer clamped-beam probe for high-sensitivity nanoforce measurements," Light. Sci. & Appl. **10**, 1–12 (2021).
25. T. A. Birks and Y. W. Li, "The shape of fiber tapers," J. Light. Technol. **10**, 432–438 (1992).
26. L. Tong, "Micro/nanofibre optical sensors: challenges and prospects," Sensors **18**, 903 (2018).
27. S. Holleis, T. Hoinkes, C. Wuttke, P. Schneeweiss, and A. Rauschenbeutel, "Experimental stress–strain analysis of tapered silica optical fibers with nanofiber waist," Appl. Phys. Lett. **104**, 163109 (2014).
28. A. Godet, A. Ndao, T. Sylvestre, V. Pecheur, S. Lebrun, G. Pauliat, J.-C. Beugnot, and K. P. Huy, "Brillouin spectroscopy of optical microfibers and nanofibers," Optica **4**, 1232–1238 (2017).
29. D. Royer and E. Dieulesaint, *Elastic waves in solids I: Free and guided propagation* (Springer Science & Business Media, 1999).
30. C. A. Galindez-Jamioy and J. M. Lopez-Higuera, "Brillouin distributed fiber sensors: an overview and applications," J. Sensors **2012** (2012).